Annals of Anatomy 223 (2019) 77–84

Contents lists available at ScienceDirect

Annals of Anatomy

journal homepage: www.elsevier.com/locate/aanat

RESEARCH ARTICLE

A novel intraoral injection technique for rat levator veli palatini muscle regeneration

Xu Cheng, Hanyao Huang, Bing Shi**, Jingtao Li*

State Key Laboratory of Oral Diseases, National Clinical Research Centre for Oral Diseases, Department of Oral and Maxillofacial Surgery, West China Hospital of Stomatology, Sichuan University, 14 Ren Min Nan Road, Chengdu, 610041, PR China

ARTICLE INFO

Article history:
Received 6 September 2018
Received in revised form 14 January 2019
Accepted 14 January 2019

Keywords:
Cleft palate
Levator veli palatini
Comparative anatomy
Wnt7a

ABSTRACT

Background: The levator veli palatini (LVP) muscle drives the elevation and retraction of the soft palate to facilitate speech and feeding, but undergoes atrophic changes in patients with cleft palate deformity. This study aimed to establish an effective drug delivery technique for LVP muscle regeneration.
Methods: An intraoral injection technique for rat LVP muscle regeneration was developed based on careful examination of the rat craniofacial anatomy. The accuracy and reliability of this technique were tested by cone-beam computed tomography and nitrocellulose dye labeling. Recombinant human Wnt7a was delivered via this injection technique, and the subsequent responses of the levator veli palatini muscle were analyzed.
Results: Both the cone-beam computed tomography orientation of the needle tip and dye labeling suggested repeatable accuracy of the injection technique. Recombinant human Wnt7a delivery via this technique induced regeneration-related changes, including increased expression of centrally nucleated myofibers and $Ki67^{+ve}$ nuclei.
Conclusion: The intraoral injection technique is safe and efficient. It can be used for accurate drug delivery and to screen regenerative therapeutics for the LVP muscle.

1. Introduction

The human palate is composed of the anterior bony hard palate and the posterior muscular soft palate. Soft palate muscles act in concert to modulate the movement of the velum and are responsible for the valvular action of the velopharyngeal sphincter, which is the foundation of speech production (Moon et al., 1994; Perry et al., 2013). Among soft palate muscles, the levator veli palatini (LVP) muscle plays the major role in velar elevation and retraction, and suspends the velum due to its sling-like structure. (Cohen et al., 1994; Koch et al., 1999; Perry et al., 2013).

Cleft palate is one of the most common congenital deformities in humans, with an occurrence of approximately 1 per 700 live births (Fallin et al., 2003; Moreau et al., 2007). In a cleft palate the palate is split in the middle and the continuity of the LVP muscle sling is interrupted (Fisher and Sommerlad, 2011). The resulting excessive air resonance and nasal air emission produces unintelligible speech. (Crockett and Goudy, 2014; Fisher and Sommerlad, 2011). Cleft palate surgeries such as "Furlow double-opposing Z-plasty" (Furlow, 1986) or "Sommerlad cleft palate repair" with radical muscle reconstruction (Sommerlad, 2003) aim to close the cleft and restore the function of soft palate muscles. Nevertheless, insufficient velopharyngeal closure and abnormal speech persist in up to 40% of post-operative patients (Gart and Gosain, 2014; Woo et al., 2014).

Surgery leads to sealing of the cleft and reconstruction of the LVP muscle sling; however, the problem of muscle deficiency is not addressed. In patients with cleft palate, the LVP muscle has a significantly reduced muscle bulk when compared to that of healthy newborns (Lazzeri et al., 2008; Carvajal Monroy et al., 2012). Moreover, the LVP muscle remains thinner in patients with a repaired cleft palate compared to that in normal controls (Ettema et al., 2002; Ha et al., 2007; Kotlarek et al., 2017). On the other hand, computational modeling studies have demonstrated that the velopharyngeal function can be improved if the LVP cross-section area is increased (Inouye et al., 2016, 2015). Thus, regeneration of the LVP to increase the muscle volume in patients with cleft palate may supplement current surgical management and improve the velopharyngeal functional component of speech.

* Corresponding author at: 14 Ren Min Nan Road, Chengdu, Sichuan, 610041, PR China.
** Corresponding author.
E-mail addresses: shibingcn@vip.sina.com (B. Shi), lijingtao86@163.com (J. Li).

https://doi.org/10.1016/j.aanat.2019.01.012
0940-9602/

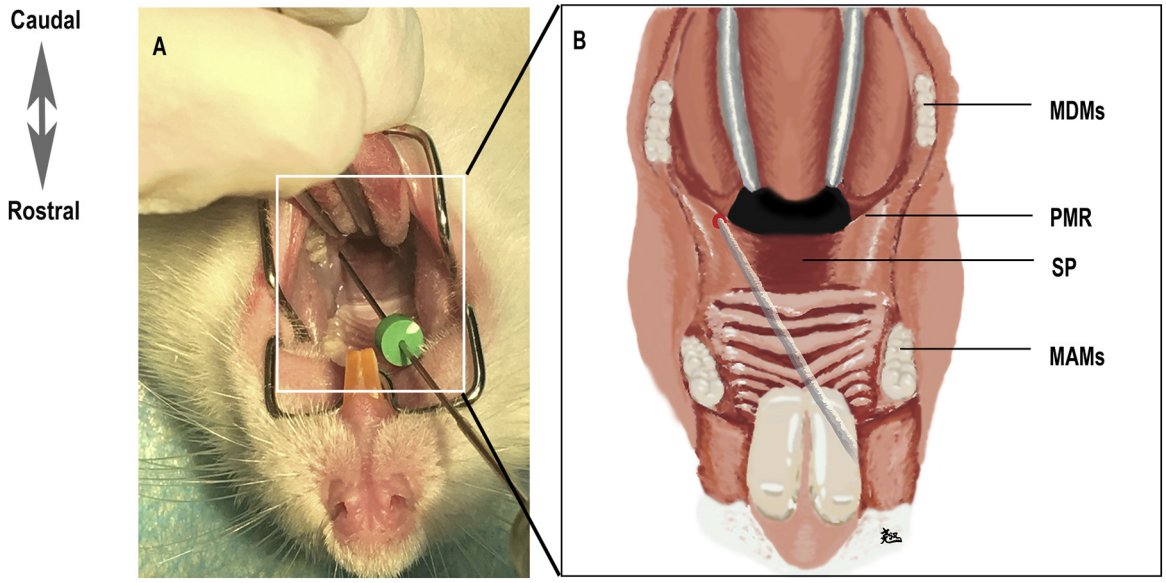

Fig. 1. Intraoral view of injection setting. (A) The photograph taken under stereoscope demonstrating the intraoral injection point. (B) Schematic representation of higher magnification. Red spot indicated the needle entry point. Abbreviations: MDMs, mandibular molars; PMR, pterygomandibular raphe; SP, soft palate; MAMs, maxillary molars. (For interpretation of the references to colour in this figure legend and in text the reader is referred to the web version of this article).

However, successful artificial muscle substitutes are not available in clinical practice, unlike substitutes for bone and skin. (Campana et al., 2014; Kolk et al., 2012; Whitaker et al., 2008; Widgerow, 2014). Various therapeutic possibilities for muscle regeneration include the potentially feasible small molecule injections. (Tabebordbar et al., 2013). An injection of recombinant human Wnt7a (rh-Wnt7a) injection can boost muscle stem cell expansion and muscle hypertrophy and can increase muscle strength. (von Maltzahn et al., 2012b) Most of these potential therapies were developed based on data acquired in limb muscle studies. Craniofacial muscles differ from limb muscles in many aspects, including their embryonic origin, myogenic regulatory pathways and the activity of the resident satellite cells.(Randolph et al., 2015; Biressi et al., 2007; Ono et al.,2010; Stuelsatz et al., 2015). Considering the differences between craniofacial muscles and limb muscles, the effectiveness of these therapeutic candidates needs to be further evaluated in craniofacial muscle models.

In contrast to the frequently employed limb muscle models such as the tibialis anterior muscle, the LVP muscle is significantly smaller and is less accessible. Thus, a method of drug delivery to the LVP muscle needs to be described in detail. In this study, we proposed a technique using an intraoral injection into the LVP muscle and confirmed the accuracy and reliability of the injection. Based on this technique, we tested the effect of rh-Wnt7a on the regenerative potential of the LVP muscle.

2. Materials and methods

2.1. Animals

Adult male Sprague-Dawley rats (10 weeks, 280–300 g) were purchased from the Dashuo Biological Technology Company, Chengdu, China. The animals were raised under standard conditions and were allowed to acclimatize for one week before being enrolled into experiments. A total of fifty-four rats were used in this study (animal distribution is listed in Table 1). All experimental procedures on the animals were in accordance with the National Institute of Health Guidelines for the Care and Use for Laboratory animals and were approved by the Institutional Animal Care and Use Committee (IACUC, protocol number: WCCSIB-D-2014-007) at West China Hospital of Stomatology, Sichuan University.

Table 1
Distribution of animals in different groups.

Treatment	Sample size	Time point analyzed
CBCT scanning	6	Immediately
Nitrocellulose dye labelling	6	Immediately
PBS injection	21	Three weeks after injection
rh-Wnt7a injection	21	Three weeks after injection

2.2. Intraoral injection technique

2.2.1. Anesthesia

Rats were anesthetized with an intramuscular injection of Zoletil 50 (Virbac S.A.) (50 mg/kg) plus atropine (Quanyu Biotechnology Co. Ltd.) (0.05 mg/kg). The sufficiency of anesthesia was assessed according to the loss of the eyelid reflex and righting reflexes (Shota et al., 2016).

2.2.2. Surgical field exposure

Rats were fixed on an operation table in supine position, and the oral cavity was accessed with the aid of a mouth gag. The tongue was suspended with a 4–0 suture to better expose the posterior part of the palate. The entire palatopharyngeal region was exposed by pressing the root of the tongue with forceps (Fig. 1A,B). Thus, the pterygomandibular raphe was clearly visible at the flank of the posterior soft palate. The midpoint of the pterygomandibular raphe was used as the entry point for a needle (Fig. 1B, indicated by red dot).

2.2.3. Intraoral injection

To control the injection depth, a stopper was placed on the needle of a 25 μl syringe approximately 13 mm away from the needle tip (Fig. 1A). Initially, the syringe was placed at an angle of approximately 30° with the midline (Injection direction 1, Fig. 2A,E). After piercing the mucosa, the needle entered the parapharyngeal space. The needle tip was pushed deeper for another 3–4 mm until it

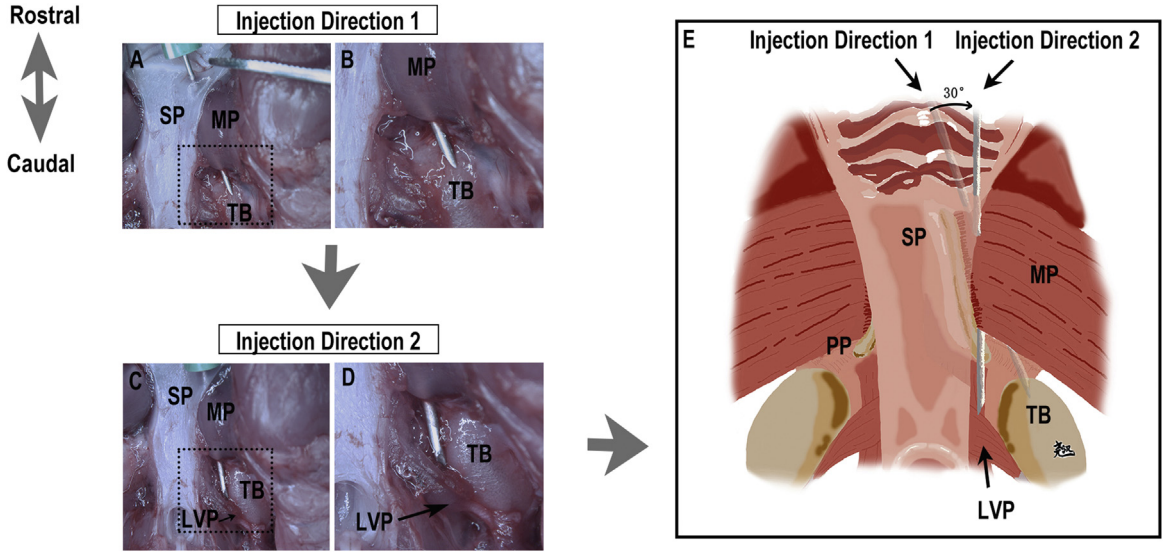

Fig. 2. Injection directions of the needle. (A) Initially the needle was placed at 30° to the midline (Injection direction 1), went through the medial pterygoid muscle and reached the tympanic bulla, with higher magnification shown in (B). (C) Then the needle was adjusted parallel to the midline (Injection direction 2) to approach the levator veli palatini muscle, with higher magnification shown in (D). (E) Schematic representation of Injection direction 1 and Injection direction 2. Abbreviations: SP, soft palate; MP, medial pterygoid muscle; TB, tympanic bulla; LVP, levator veli palatini muscle; PP, pterygoid process.

engaged a bony structure, the tympanic bulla (Injection direction 1, Fig. 2B,E). Then, the needle was disengaged from the bony surface, and the syringe position was adjusted in parallel with the midline (Injection direction 2, Fig. 2C,E). Then, the needle was moved caudally for another 2 mm to approximate the LVP muscle (Injection direction 2, Fig. 2D,E). At this point, the injection was slowly performed.

2.2.4. Resuscitation

When the injection was complete, the rats were kept on a heater plate maintained at approximately 38 °C. The animals were observed every 10 min until the righting reflex recovered.

2.3. Cone-beam computed tomography

Six rats underwent cone-beam computed tomography (CBCT) scanning (J. Morita MFG Corp., Kyoto, Japan) with a needle in the injection position. Rats were fixed in supine position, and the standard scanning program (scan time 17.5 s, FOV 140 × 100 mm) was applied. Coronal, sagittal and transverse images were extracted to estimate the relative position of the needle tip versus the tympanic bulla in One Data Viewer software (Morita Manufacturing Corp.). Images were remodeled by the medical image processing software (Mimics, Materialise).

2.4. Nitrocellulose dye labelling

The injection site was labeled by a blue nitrocellulose dye. Six rats were euthanized and injected with 25 μl nitrocellulose dye using the technique described above. Careful dissection was performed immediately after the injection to locate the blue-dyed area.

2.5. Rh-Wnt7a delivery

After confirming the accuracy and reliability of the LVP muscle injection technique, the rh-Wnt7a protein was delivered to explore its effect on the LVP muscle. In the experimental group (N = 21), 25 μl (100 μg/ml) rh-Wnt7a was injected in the left LVP muscle in each rat, and in the control group (N = 21), an equal volume of sterilized phosphate-buffered saline (PBS) was injected in the left LVP muscle in each rat.

2.6. LVP muscle dissection

The LVP muscle was dissected as described with Carvajal Monroy (Carvajal Monroy et al., 2013) with some modifications. A ventral skin incision extending from the mandibular symphysis to the clavicle was made, and subcutaneous tissue was separated to expose the submandibular gland. After removal of the salivary gland, the posterior digastric muscle and sternocleidomastoid muscle were exposed (Fig. 3A,D). The posterior belly of the digastric muscle was bluntly dissected down to its attachment to the tympanic bulla. The digastric muscle was transected at the central tendon and pulled aside to expose the stylohyoid muscle (Fig. 3B,E). The stylohyoid muscle was released at its attachment point to the hyoid and the LVP muscle was exposed with its tendon attached to the tympanic bulla. The LVP muscle runs medially and rostrally and is attached to the soft palate (Fig. 3C,F). During muscle dissection, images were acquired with a Zeiss SteoREO Discovery V20 microscope. Images were captured using an Olympus BX63 immunofluorescence microscope.

2.7. Immunohistochemistry

Muscle samples were embedded with Optimal Cutting Temperature compound (tissue-tech) and frozen in isopentane cooled with liquid nitrogen using Meng's method (Meng et al., 2014). Cryosections were fixed in ice-cold acetone and washed in 0.01 mol/l PBS. Sections were blocked with PBS containing 5% bovine serum albumin and 5% donkey serum for 1 h at room temperature, and subsequently incubated overnight at 4 °C with anti-laminin primary antibody (1:1000, L9393, Sigma-Aldrich) and anti-Ki67 primary antibody (1:500, ab16667, Abcam). Following washing in PBS, sections were incubated for 1 h at room temperature with Alexa Fluor 488-conjugated and 568-conjugated secondary antibodies. After several washes in PBS, the nuclei were stained with DAPI (D9542, Sigma). Images were captured under Olympus BX63 immunofluorescence microscope.

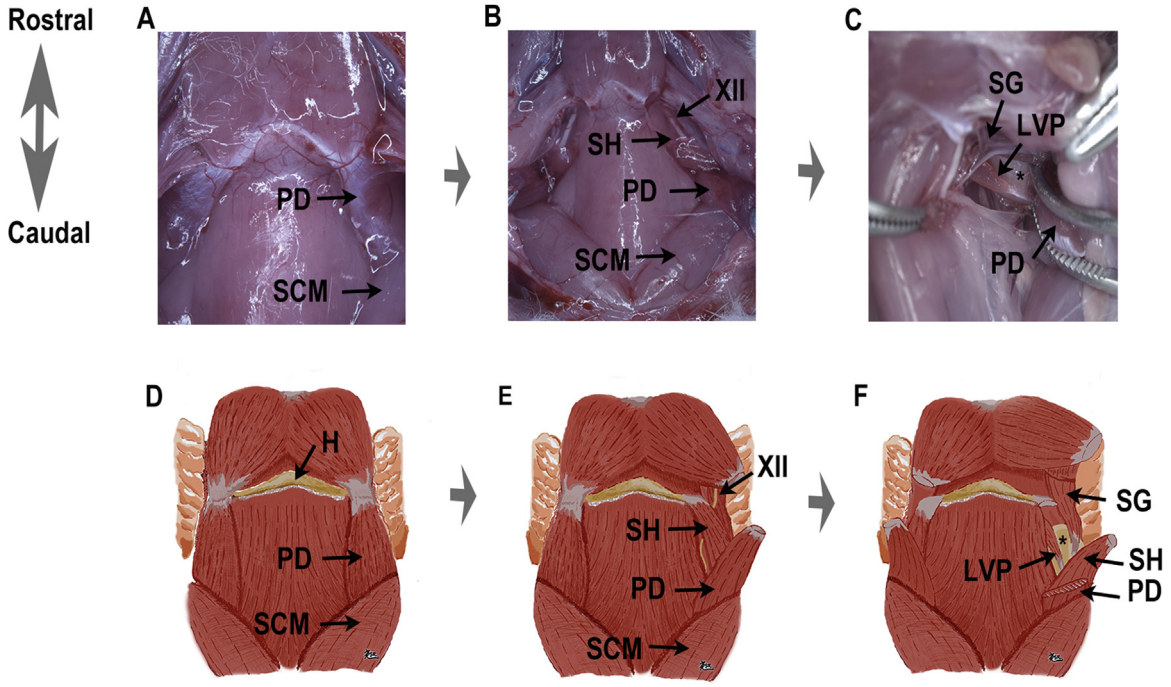

Fig. 3. Illustration of levator veli palatini muscle dissection. (A, D) The posterior digastric muscle and the sternocleidomastoid muscle were exposed after removing the salivary gland. (B, E) The digastric muscle was transected at the central tendon and pulled aside to expose the stylohyoid muscle. The hypoglossal nerve could be seen adjacent to the stylohyoid muscle. (C, F) The stylohyoid muscle was released at its attachment to the hyoid and the LVP muscle became visible. The LVP muscle was closely attached to the tympanic bulla, with the styloglossus muscle running alongside. The styloglossus muscle was removed in (C) to facilitate visualization of the LVP muscle. Black asterisk indicated the tympanic bulla. H: hyoid bone, PD: posterior digastric muscle, SCM: sternocleidomastoid muscle, SH: stylohyoid muscle, SG: styloglossus muscle, LVP: levator veli palatini muscle, XII: hypoglossal nerve.

2.8. Sample size calculation

Sample size calculation was conducted by power analysis (Charan and Kantharia, 2013; Noordzij et al., 2011). Type I error was set at 0.05 and type II error was set at 0.2. Effect size was calculated according to a pilot study. The sample size was then calculated by G*power (Faul et al., 2007) to be 42 in total: 21 in PBS-treated group and 21 in rh-Wnt7a-treated group.

2.9. Statistical analysis

The number of total myofibers, centrally nucleated myofibers, total nuclei and Ki67^{+ve} nuclei were counted with Image J software. All data were analyzed using SPSS 19.0 (Inc., Chicago, IL, USA). One-sample Kolmogorov–Smirnov test revealed that the data was normally distributed. Then the average percentage of Ki67^{+ve} nuclei and centrally nucleated myofibers among PBS-treated and rh-Wnt7a-treated groups were compared using independent-samples *t* test. The results were expressed as Mean ± SEM.

3. Results

3.1. The tympanic bulla was a reliable marker for guiding the intraoral injection

The intraoral LVP muscle injection technique described in the present study was developed after a meticulous investigation of the rat craniofacial anatomy (Figs. 1–3). The tympanic bulla was proposed as an important marker for guiding the needle to the LVP muscle. To test the reliability of this injection technique, six rats were intraorally punctured with syringe needles as described in Section "2"- Section 2.2.2 and 2.2.3. Then, the animals were subjected to CBCT scanning with the needle in place. The needle tip was visualized due to its high density, while the tympanic bulla was detected as a high-density circle containing air in the middle. The needle tip was adjacent to the tympanic bulla in the coronal, sagittal and transverse planes of the CBCT images (Fig. 4A,B,C). The distances from the needle tip to the medial and caudal poles of the tympanic bulla were measured (Fig. 4D). The distance to the medial pole was 1.48 ± 0.64 mm, and the distance to caudal pole was 4.80 ± 0.54 mm. The distances were measured in each individual rat and plotted in the diagram (Fig. 4E). For all six punctures, the needle tip reached the medial rostral aspect of the tympanic bulla (Fig. 4F), demonstrating satisfactory repeatability.

3.2. The LVP muscle was accurately accessed via the intraoral injection technique

We further tested the efficiency of the delivery of injectable substances to the surface of the LVP muscles via the intraoral technique. The blue-colored dye was easily spotted, and the hydrophobicity of the dye prevented diffusion, thus accurately labeling the injection site. In all six rats injected with the blue dye, the LVP muscle was stained blue (Fig.4 G,H). The accuracy of the LVP muscle injection was thus confirmed.

3.3. Rh-Wnt7a injection increased the percentage of centrally nucleated myofibers and proliferation activity in the LVP muscle

Centrally nucleated myofibers (CNMs) are markers of muscle renewal and regeneration (Keefe et al., 2015). In resting condition, the expression of CNMs in mature muscles was low, as shown in our previous study (Cheng et al., 2017). Three weeks after injection, the CNMs percentage in the Wnt7a group was 22.76 ± 2.64% (Fig. 5A–E), corresponding to an approximately seven-fold increase compared to the PBS-treated group ($p < 0.001$). Similarly, the expression level of the Ki67^{+ve} nuclei was significantly higher in the Wnt7a group than that in the PBS group ($p < 0.001$) (Fig. 5F–J). These data

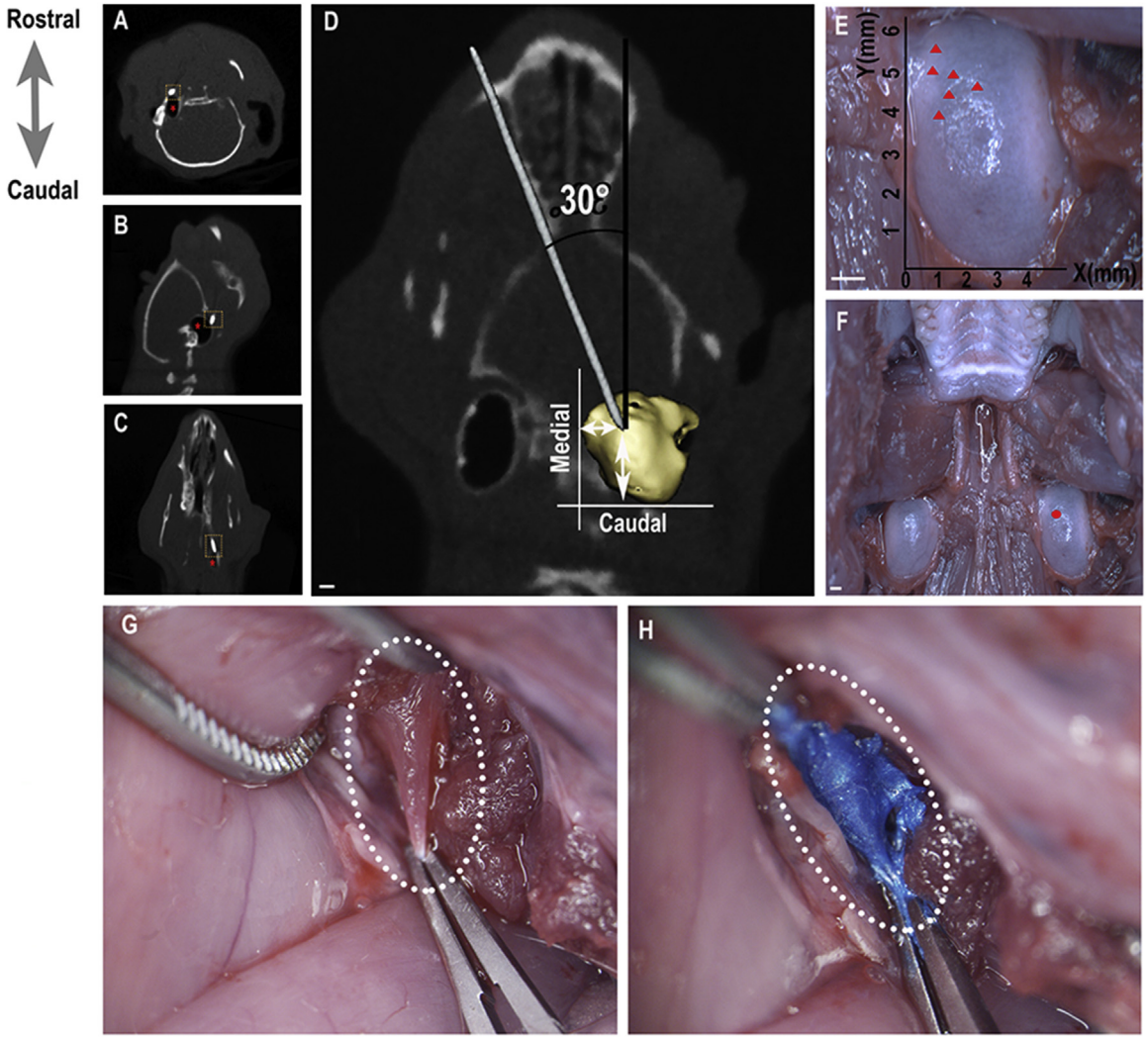

Fig. 4. Accuracy test of the intraoral injection technique. CBCT images of transverse (A), sagittal (B) and coronal (C) anatomical plane. The high density point inside the yellow dotted area indicated needle tip. Red asterisk represented tympanic bulla. (D) Remodeled image of CBCT scanning with schematic illustration of distance measurement. The distances from needle tip to the medial and caudal aspect of tympanic bulla were measured. (E) Gross view of tympanic bulla. X and Y referred to distance from needle tip to the medial and caudal pole of tympanic bulla, respectively. Distances measured in each individual rat were plotted in the scatter diagram. (F) Gross view of the posterior part of rat mouth with soft palate and its affiliated muscles removed. The red spot represented the average value calculated from distance X and Y. (G) Stereoscopic image of the LVP muscle without injection. (H) Stereoscopic image of the LVP muscle after nitrocellulose blue dye delivery. Scale bar = 1 mm. (For interpretation of the references to colour in this figure legend and in text the reader is referred to the web version of this article).

indicated that the rh-Wnt7a injection induced active myofiber production in the LVP muscle.

4. Discussion

The intraoral LVP muscle injection technique was found to be safe and effective in the present study. All rats survived the injection procedure. Surgical bleeding occurred in seven of the fifty-four injections and was successfully controlled by applying pressure with a cotton swab. This bleeding was likely due to a deviation of the injection direction, which caused damage to the pterygoid venous plexus. Strict control of the insertion angle is required to avoid excessive bleeding.

The anatomy and histology of the rat soft palate is essentially similar to those of humans (Carvajal Monroy et al., 2013). Five muscles compose the soft palate: the palatopharyngeus, the palatoglossus, the tensor veli palatini, the musculus uvulae, and the LVP. The LVP muscle was chosen as the study subject over the entire soft palate musculature for two major reasons: (1) The LVP muscle is the major contributor to the velum elevation (Perry et al., 2013, 2014), and an increase in the muscle volume of the LVP can effectively improve the velopharyngeal function (Inouye et al., 2016, 2015); (2) The muscles in the soft palate spread into various directions; thus existing technologies cannot capture the transverse section of all muscles at the same time to quantitatively analyze the myofibers (Carvajal Monroy et al., 2013, 2012). The main determinants of the architectural characteristics of the muscle requires quantification, including the fiber diameter and fiber type distribution (Narici et al., 2016). In this study, the LVP muscle was isolated and dissected as a cylindrical muscle bundle, thus facilitating the quantification of these structural determinants of the muscle.

Another benefit of this study includes the detection of three muscle layers during the dissection of the rat LVP muscle. The posterior digastric muscle and the sternocleidomastoid muscle form the superficial muscle layer. The intermediate muscle layer is occupied by the stylohyoid muscle, which is located beneath the posterior digastric muscle. The volume of the stylohyoid muscle is significantly higher and it totally covers the LVP muscle. The LVP muscle can only be visualized after the stylohyoid muscle is

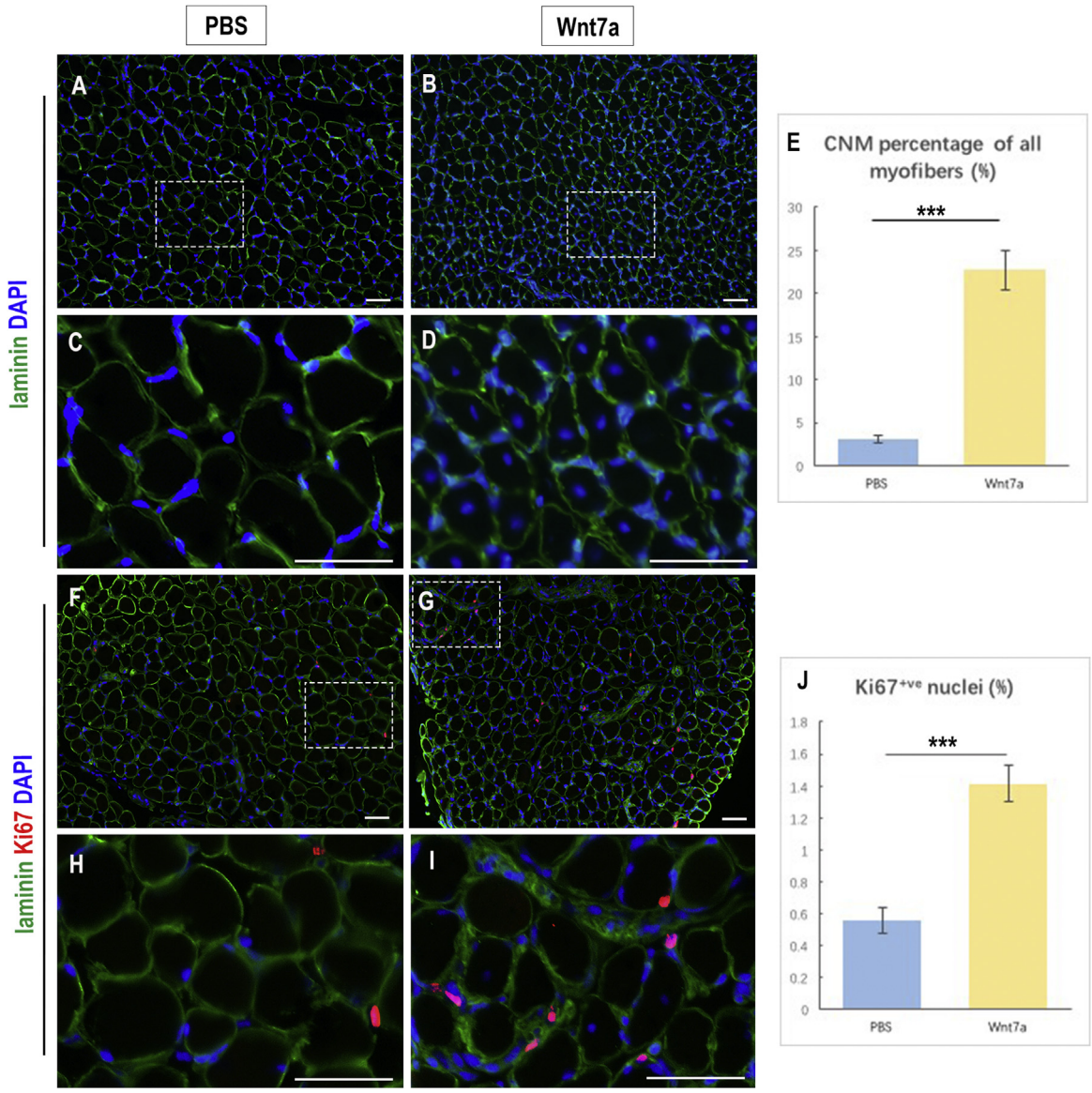

Fig. 5. Rh-wnt7a delivery via intraoral injection technique led to regeneration-related activities in the levator veli palatini muscle. (A–D) Immunofluorescence staining of laminin (green) and DAPI (blue) in the LVP muscle treated with PBS or rh-Wnt7a. (E) Quantification of centrally nucleated myofibers. (F–I) Immunofluorescence staining of laminin (green), Ki67 (red) and DAPI (blue) in the LVP muscle treated with PBS or rh-Wnt7a. (J) Quantification of Ki67^{+ve} nuclei. CNMs: centrally nucleated myofibers. Scale bar = 50um; ***, $p < 0.001$. (For interpretation of the references to colour in this figure legend and in text the reader is referred to the web version of this article).

pulled in lateral direction. The LVP muscle runs medially and rostrally to enter the soft palate, and the parallel styloglossus muscle runs rostrally and joins the tongue muscles. The LVP muscle and the styloglossus muscle compose the third muscle layer and are attached adjacent to the surface of the tympanic bulla. Clarification of the anatomy and development of the dissection technique are required for in-depth study of the LVP muscle.

Previous studies by Rudnicki (von Maltzahn et al., 2012a,b; Le Grand et al., 2009; Rudnicki and Williams, 2019) demonstrated that rh-Wnt7a injected into the hind limb of mice triggered vigorous muscle regeneration. Thus, rh-Wnt7a was considered a potent muscle growth factor. Nevertheless, craniofacial muscles differed from their limb muscles in many aspects, including the embryonic origin (Sambasivan et al., 2011), the myogenic regulatory pathways (Noden and Francis-West, 2006), the muscle proliferation capacity (Ono et al., 2010) and the satellite cell activity (Randolph et al., 2015). In particular, pharyngeal muscles have been shown to undergo myonuclear turnover more frequently than hind limb muscles (Randolph et al., 2015). Thus it is unclear whether the growth factors that are effective in limb muscles would work in a similar manner in the muscles of the craniofacial region. In this study, rh-Wnt7a injected in the LVP muscle significantly increased the percentage of CNMs, similar to the effect of rh-Wnt7a in limb muscles (von Maltzahn et al., 2012a,b). An increase in the Ki67^{+ve} nuclei after rh-Wnt7a administration indicated enhanced muscle proliferation, which was not found in previous studies. Additional insight into the biological mechanism of these effects will require further study.

This study has several limitations. First, muscle regeneration processes typically involve myofiber necrosis (Grounds, 2014), which was not investigated in our study; the increased expression of CNMs and Ki67^{+ve} nuclei can be more accurately referred to as a muscle regeneration-related phenotype rather than muscle regeneration. To characterize the specific regenerative effect of rh-Wnt7a on the LVP, an injury model should be employed. Second, the injection technique used in this study induced changes in other regions in addition to the LVP. The Styloglossus also demonstrated an increased percentage of CNMs (Fig. A.1) due to its close

relationship with the LVP, although the increase was significantly smaller. Third, the ultimate purpose of the LVP muscle regeneration is to enhance the elevation capacity of the soft palate (Inouye et al., 2016, 2015; von Maltzahn et al., 2012b,b). Thus, functional tests of the LVP after rh-Wnt7a delivery are imperative in future studies.

5. Conclusion

The intraoral injection technique described here was used for accurate drug delivery to and screening of regenerative therapeutics in the levator veli palatini muscle. Rh-Wnt7a delivered via this injection technique effectively triggered regeneration-related activities in the levator veli palatini muscle.

Funding

This study was supported by grants from the National Natural Science Foundation of China to Dr. Jingtao Li (Grant Number: 81500829) and Dr. Bing Shi (Grant Number: 81470729).

Ethical statement

All experimental procedures on animals were in accordance with National Institute of Health Guidelines for the Care and Use for Laboratory animals and were approved by the Institutional Animal Care and Use Committee (IACUC, protocol number: WCCSIB-D-2014-007) at West China Hospital of Stomatology, Sichuan University.

CRediT authorship contribution statement

Xu Cheng: Investigation, Methodology, Data curation, Data curation, Formal analysis. **Hanyao Huang:** Formal analysis, Resources, Software, Visualization. **Bing Shi:** Conceptualization, Funding acquisition, Project administration, Supervision. **Jingtao Li:** Conceptualization, Funding acquisition, Data curation, Project administration, Validation, Supervision, Writing - review & editing.

Acknowledgements

The authors would like to acknowledge Xiaoxiao Pang and Lei Song (West China School of Stomatology, Sichuan University) for assistance with data collection and immunohistochemistry procedures.

References

Biressi, S., Molinaro, M., Cossu, G., 2007. Cellular heterogeneity during vertebrate skeletal muscle development. Dev. Biol. (Basel) 308, 281–293, http://dx.doi.org/10.1016/j.ydbio.2007.06.006.

Campana, V., Milano, G., Pagano, E., Barba, M., Cicione, C., Salonna, G., Lattanzi, W., Logroscino, G., 2014. Bone substitutes in orthopaedic surgery: from basic science to clinical practice. J. Mater. Sci. Mater. Med. 25, 2445–2461, http://dx.doi.org/10.1007/s10856-014-5240-2.

Carvajal Monroy, P.L., Grefte, S., Kuijpers-Jagtman, A.M., Wagener, F.A.D.T.G., V. den, H.J., 2012. Strategies to improve regeneration of the soft palate muscles after cleft palate repair. Tissue Eng. B-Rev. 18, 468–477, http://dx.doi.org/10.1089/ten.teb.2012.0049.

Carvajal Monroy, P.L., Grefte, S., Kuijpers-Jagtman, A.M., Helmich, M.P.A.C., Ulrich, D.J.O., Von den Hoff, J.W., W.F.A.D.T, 2013. A rat model for muscle regeneration in the soft palate. PLoS One 8, e59193, http://dx.doi.org/10.1371/journal.pone.0059193.

Charan, J., Kantharia, N., 2013. How to calculate sample size in animal studies? J. Pharmacol. Pharmacother. 4, 303, http://dx.doi.org/10.4103/0976-500X.119726.

Cheng, X., Song, L., Lan, M., Shi, B., Jingtao, L., Li, J., 2017. Morphological and molecular comparisons between tibialis anterior muscle and levator veli palatini muscle: a preliminary study on their augmentation potential. Exp. Ther. Med. 15, 247–253, http://dx.doi.org/10.3892/etm.2017.5391.

Crockett, D.J., Goudy, S.L., 2014. Update on surgery for velopharyngeal dysfunction. Curr. Opin. Otolaryngol. Head Neck Surg. 22, 267–275, http://dx.doi.org/10.1097/MOO.0000000000000063.

Cohen, S.R., Chen, L., Burdi, A.R., Trotman, C.A., 1994. Patterns of Abnormal Myogenesis in Human Cleft Palates. Cleft Palate Craniofac. J. 31, 345–350.

Ettema, S.L., Kuehn, D.P., Perlman, A.L., Alperin, N., 2002. Magnetic resonance imaging of the levator veli palatini muscle during speech. Cleft Palate Craniofac. J. 39, 130–144, http://dx.doi.org/10.1597/1545-1569(2002)039<0130:MRIOTL>2.0.CO;2.

Fallin, M.D., Hetmanski, J.B., Park, J., Scott, A.F., Ingersoll, R., Fuernkranz, H.A., McIntosh, I., Beaty, T.H., 2003. Family-based analysis of MSX1 haplotypes for association with oral clefts. Genet. Epidemiol. (25), 168–175, http://dx.doi.org/10.1002/gepi.10255.

Faul, F., Erdfelder, E., Lang, A.-G., Buchner, A., 2007. G*Power: a flexible statistical power analysis program for the social, behavioral, and biomedical sciences. Behav. Res. Methods 39, 175–191, http://dx.doi.org/10.3758/BF03193146.

Fisher, D.M., Sommerlad, B.C., 2011. Cleft lip, cleft palate, and velopharyngeal insufficiency. Plast. Reconstr. Surg. 128, 342e–360e, http://dx.doi.org/10.1097/PRS.0b013e3182268e1b.

Furlow, L.T.J., 1986. Cleft palate repair by double opposing Z-plasty. Plast. Reconstr. Surg. (78), 724–738.

Gart, M.S., Gosain, A.K., 2014. Surgical management of velopharyngeal insufficiency. Clin. Plast. Surg. 41, 253–270, http://dx.doi.org/10.1016/j.cps.2013.12.010.

Grounds, M.D., 2014. The need to more precisely define aspects of skeletal muscle regeneration. Int. J. Biochem. Cell Biol. 56, 56–65, http://dx.doi.org/10.1016/j.biocel.2014.09.010.

Ha, S., Kuehn, D.P., Cohen, M., A.N, 2007. Magnetic resonance imaging of the levator veli palatini muscle in speakers with repaired cleft palate. Cleft Palate Craniofac. J. 44, 494–505, http://dx.doi.org/10.1597/06-220.1.

Inouye, Johanne M., Perry, J.L., Lin, K.Y., Blemker, S.S., 2015. The development of english as a second language with and without specific language impairment: clinical implications. J. Speech Lang. Hear. Res. 24, 1–14, http://dx.doi.org/10.1044/2015.

Inouye, J.M., Lin, K.Y., Perry, J.L., Blemker, S.S., 2016. Contributions of the musculus uvulae to velopharyngeal closure quantified with a 3-dimensional multimuscle computational model. Ann. Plast. Surg. 77, 70–75, http://dx.doi.org/10.1097/SAP.0000000000000777.

Keefe, A.C., Lawson, J.A., Flygare, S.D., Fox, Z.D., Colasanto, M.P., Mathew, S.J., Yandell, M., K.G, 2015. Muscle stem cells contribute to myofibres in sedentary adult mice. Nat. Commun. 6, 1–11, http://dx.doi.org/10.1038/ncomms8087.

Koch, K.H.H., Grzonka, M.A., Koch, J., 1999. The pathology of velopharyngeal musculature in cleft palates. Ann. Anat. 181, 123–126.

Kolk, A., Handschel, J., Drescher, W., Rothamel, D., Kloss, F., Blessmann, M., Heiland, M., Wolff, K.D., Smeets, R., 2012. Current trends and future perspectives of bone substitute materials - from space holders to innovative biomaterials. J. Craniomaxillofac. Surg. 40, 706–718, http://dx.doi.org/10.1016/j.jcms.2012.01.002.

Kotlarek, K.J., Perry, P.L., F.X, 2017. Morphology of the Levator Veli Palatini Muscle in Adults With Repaired Cleft Palate. J. Craniofac. Surg. 28, 833–837, http://dx.doi.org/10.1097/SCS.0000000000003373.

Lazzeri, D., Viacava, P., Pollina, L.E., Sansevero, S., Lorenzetti, F., Balmelli, B., Funel, N., Gatti, G.L., Naccarato, A.G., Massei, A., 2008. Dystrophic-like alterations characterize orbicularis oris and palatopharyngeal muscles in patients affected by cleft lip and palate. Cleft Palate Craniofac. J. 45, 587–591, http://dx.doi.org/10.1597/07-026.1.

Le Grand, F., Jones, A.E., Seale, V., Scime, A., R.M, 2009. Wnt7a activates the planar cell polarity pathway to drive the symmetric expansion of satellite stem cells. Cell Stem Cell 4, 535–547, http://dx.doi.org/10.1016/j.stem.2009.03.013.

Meng, H., Janssen, P.M.L., Grange, R.W., Yang, L., Beggs, A.H., Swanson, L.C., Cossette, S.A., Frase, A., Childers, M.K., Granzier, H., Gussoni, E., L.M, 2014. Tissue triage and freezing for models of skeletal muscle disease. J. Vis. Exp., e51586, http://dx.doi.org/10.3791/51586.

Moon, J.B., Smith, A.E., Folkins, J.W., Lemke, J.H., Gartlan, M., 1994. Coordination of velopharyngeal muscle activity during positioning of the soft palate. Cleft Palate Craniofacial J., http://dx.doi.org/10.1597/1545-1569_1994_031_0045_covmad_2.3.co_2.

Moreau, J.L., Caccamese, J.F., Coletti, D.P., Sauk, J.J., Fisher, J.P., 2007. Tissue engineering solutions for cleft palates. J. Oral Maxillofac. Surg. 65, 2503–2511, http://dx.doi.org/10.1016/j.joms.2007.06.648.

Narici, M., Franchi, M., Maganaris, C., 2016. Muscle structural assembly and functional consequences. J. Exp. Biol. 219, 276–284, http://dx.doi.org/10.1242/jeb.128017.

Noden, D.M., Francis-West, P., 2006. The differentiation and morphogenesis of craniofacial muscles. Dev. Dyn. 235, 1194–1218, http://dx.doi.org/10.1002/dvdy.20697.

Noordzij, M., Dekker, F.W., Zoccali, C., Jager, K.J., 2011. Sample size calculations. Nephron Clin. Pract. 118, 319–323, http://dx.doi.org/10.1159/000322830.

Ono, Y., Boldrin, L., Knopp, P., Morgan, J.E., Z.P, 2010. Muscle satellite cells are a functionally heterogeneous population in both somite-derived and branchiomeric muscles. Dev. Biol. (Basel) 337, 29–41, http://dx.doi.org/10.1016/j.ydbio.2009.10.005.

Perry, J.L., Kuehn, D.P., Sutton, B.P., 2013. Morphology of the levator veli palatini muscle using magnetic resonance imaging. Cleft Palate Craniofac. J. 50, 64–75, http://dx.doi.org/10.1597/11-125.

Perry, J.L., Kuehn, D.P., Sutton, B.P., Gamage, J.K., 2014. Sexual dimorphism of the levator veli palatini muscle: an imaging study. Cleft Palate Craniofac. J. 51, 544–552, http://dx.doi.org/10.1597/12-128.

Randolph, M.E., Phillips, B.L., Choo, H.J., Vest, K.E., Vera, Y., P.G, 2015. Pharyngeal satellite cells undergo myogenesis under basal conditions and are required for pharyngeal muscle maintenance. Stem Cells 33, 3581–3595, http://dx.doi.org/10.1002/stem.2098.

Rudnicki, M.A., Williams, B.O., 2015. Wnt signaling in bone and muscle. Bone 80, 60–66, http://dx.doi.org/10.1016/j.bone.2015.02.009.

Sambasivan, R., Kuratani, S., T.S, 2011. An eye on the head: the development and evolution of craniofacial muscles. Development 138, 2401–2415, http://dx.doi.org/10.1242/dev.040972.

Shota, Higuchi, Riku, Yamada, Asami, Hashimoto, Kenjiro, Miyoushi, Kazuto, Yamashita, Takeo, O., 2016. Evaluation of a combination of alfaxalone with medetomidine and butorphanol for inducing surgical anesthesia in laboratory mice. Jpn. J. Vet. Res. 64, 131–139, http://dx.doi.org/10.14943/jjvr.64.2.131.

Sommerlad, B.C., 2003. A technique for cleft palate repair. Plast. Reconstr. Surg. 112, 1542–1548, http://dx.doi.org/10.1097/01.PRS.0000085599.84458.D2.

Stuelsatz, P., Shearer, A., Li, Y., Muir, L.A., Ieronimakis, N., Shen, Q.W., Kirillova, I., Yablonka-Reuveni, Z., 2015. Extraocular muscle satellite cells are high performance myo-engines retaining efficient regenerative capacity in dystrophin deficiency. Dev. Biol. (Basel) 397, 31–44, http://dx.doi.org/10.1016/j.ydbio.2014.08.035.

Tabebordbar, M., Wang, E.T., W.A, 2013. Skeletal muscle degenerative diseases and strategies for therapeutic muscle repair. Annu. Rev. Pathol. 8, 441–475, http://dx.doi.org/10.1146/annurev-pathol-011811-132450.

von Maltzahn, J., Bentzinger, C.F., R, M., 2012a. Wnt7a-Fzd7 signalling directly activates the Akt/mTOR anabolic growth pathway in skeletal muscle. Nat. Cell Biol. 14, 186–191, http://dx.doi.org/10.1038/ncb2404.

von Maltzahn, J., Renaud, J.M., Parise, G., Rudnicki, M.A., 2012b. Wnt7a treatment ameliorates muscular dystrophy. Proc Natl Acad Sci U S A 109, 20614–20619, http://dx.doi.org/10.1073/pnas.1215765109.

Whitaker, I.S., Prowse, S., Potokar, T.S., 2008. A critical evaluation of the use of biobrane as a biologic skin substitute. Ann. Plast. Surg. 60, 333–337, http://dx.doi.org/10.1097/SAP.0b013e31806bf446.

Widgerow, A.D., 2014. Bioengineered skin substitute considerations in the diabetic foot ulcer. Ann. Plast. Surg. 73, 239–244, http://dx.doi.org/10.1097/SAP.0b013e31826eac22.

Woo, A.S., Skolnick, G.B., Sachanandani, N.S., Grames, L.M., 2014. Evaluation of two palatal repair techniques for the surgical management of velopharyngeal insufficiency. Plast. Reconstr. Surg. 134, 588e–596e, http://dx.doi.org/10.1097/PRS.0000000000000506.